Available online at www.sciencedirect.com

ScienceDirect

journal homepage: www.intl.elsevierhealth.com/journals/dema

Metal release from ceramic coatings for dental implants

M. Mohedano, E. Matykina, R. Arrabal, A. Pardo, M.C. Merino*

Departamento de Ciencia de Materiales, Facultad de Ciencias Químicas, Universidad Complutense, 28040 Madrid, Spain

ARTICLE INFO

Article history:
Received 16 July 2013
Received in revised form
9 December 2013
Accepted 17 December 2013

Keywords:
Plasma electrolytic oxidation
Titanium
Bioactive coatings
Metal release
Simulated body fluid

ABSTRACT

Objectives. Two types of ceramic coatings on commercially pure titanium for dental implant applications with different Ca/P ratios in the range from 1.5 to 4.0, and two different thicknesses (~5 and ~15 μm) were examined with the aim of underpinning the effect of coating composition, thickness and microstructure on the corrosion behavior and hydroxyapatite forming ability in SBF.

Methods. Bioactive coatings were formed on Ti by plasma electrolytic oxidation (PEO). The composition, structure, and morphology of the materials were characterized before and after the immersion in simulated body fluid solution (SBF) at 37 °C for up to 4 weeks. All the materials were screened with respect to metal ion release into SBF.

Results. Only thick PEO coating with overstoichiometric Ca/P ratio of 4.0 exhibited capacity to induce the precipitation of hydroxyapatite over the short period of 1 week. Long term Ti^{4+} ion release from all PEO-coated materials was 2–3 times lower than from the uncoated Ti. Metal ion release is attributed mostly to chemical dissolution of the coating at initial stages of immersion.

Significance. The long term stability was greater for thin PEO coating with overstoichiometric Ca/P ratio of 2.0, which exhibited ~95 ng cm^{-2} of Ti^{4+} ions release over 4 weeks. Thin PEO coatings present economically more viable option.

1. Introduction

Titanium and its alloys are well known as artificial biomaterials used for manufacturing of dental and orthopedic implants due to their high corrosion resistance and good mechanical stability [1,2]. Their biocompatibility is related to the chemical stability and structural integrity of the surface oxide layer (TiO_2) [3]. However, the thin native oxide layer does not form a strong bond with human bones since it is bio-inert [4].To overcome this drawback, the structure, composition, and chemistry of the titanium surface needs to be modified [5–7].

Plasma electrolytic oxidation (PEO), also known as micro-arc oxidation (MAO), is a relative newcomer in the biomedical field, a convenient technique for forming porous ceramic-like bioactive coatings on surfaces of titanium [8–10]. The porous oxide layers containing a mixture of anatase and rutile as well as bioactive elements, such as Ca, P, Si, Mg and Ag originating from the electrolyte, accelerate calcium phosphate formation on their surface in simulated body fluid (SBF) and promote the formation of hydroxyapatite (HA) [11–15]. A further advantage of PEO coatings is their good adhesion, since coating formation involves conversion (oxidation) of the substrate [16,17]. In addition, both *in vitro* [18] and *in vivo* [19] evaluations have revealed that PEO treatment considerably improves the bioactivity of titanium [20] and results in accelerated osseointegration of an implant. The latter is being

* *Corresponding author*. Tel.: +34 91 394 4354; fax: +34 91 394 4356.
E-mail addresses: ematykin@ucm.es, endge@hotmail.co.uk (E. Matykina).
0109-5641/$ – see front matter © 2013 Academy of Dental Materials. Published by Elsevier Ltd. All rights reserved.
http://dx.doi.org/10.1016/j.dental.2013.12.011

Table 1 – Typical physiological media.

Material	Physiological solution	Reference
Ti6 A4lV	SBF	[38]
Ti–23Nb–0.7Ta–2Zr–O	Ringer's solution	[39]
Ti6Al4V and Ti6Al6Nb	Hank's balanced salt solution	[40]
Ti–6Al–4V and Ti–6Al–7Nb	Hank's naturally aerated solution	[41]
Ti–Mo	Fluoridated physiological serum	[42]
Ti CP, Ti6 A4lV and Ti-15Mo	Ringer's solution	[43]
Ti–6Al–4V	SBF	[44]
Ti	Ringer's solution	[45]
Ti	Artificial saliva	[46]
Ti	Artificial saliva	[47]
Ti	Fusayama and Meyer's artificial saliva	[48]
Ti–0.5Si–0.65C	Phosphate buffered saline	[49]
Sinteredporous Ti–10Mo	SBF	[50]
Ti–6Al–4V	Ringer's solution	[51]

attributed to specific topography of PEO coatings as well as to the presence of Ca and P in their composition. Since one of the characteristics of the bioactivity of a metallic implant for bone reconstruction is its apatite-forming ability in simulated body fluid, latest research on bioactive PEO coatings focuses in the generation of HA or compounds which act as precursors of HA using one-step approach, where Ca–P phases are generated during PEO, or involving post-treatments [21–30].

One of the most important characteristics of an implant is its service life, which must be extended as long as possible. This will largely depend on the corrosion resistance of the metal implant material and the release of metal ions: these are the critical factors that can adversely affect the mechanical integrity and biocompatibility [31–33]. It has been reported that the stability of the titanium surface oxide layer may be affected in physiological environments *in vivo* [34], increasing the metal ion release. This has been a source of concern due to potentially harmful effect of Ti^{4+} ions *in vivo*, because they have been shown to affect both proliferation and synthesis of extracellular matrix *in vitro* [35–37]. Therefore, the electrochemical behavior of titanium and its alloys in biological media is of increasing interest.

Table 2 – Composition per litre of the immersion solution.

Reagents	Purity (%)	m-SBF[a]
NaCl	>99.5	5.403 g
$NaHCO_3$	>99.5	0.504 g
Na_2CO_3	>99.5	0.426 g
KCl	>99.5	0.225 g
$K_2HPO_4{\cdot}3H_2O$	>99.0	0.230 g
$MgCl_2{\cdot}6H_2O$	>98.0	0.311 g
0.2 M–NaOH	–	100 mL[b]
HEPES[c]	>99.9	17.892 g[b]
$CaCl_2$	>95.0	0.293 g
Na_2SO_4	>99.0	0.072 g
1.0 M–NaOH	–	15 mL

[c] HEPES = 2-(4-(2-hydroxyethyl)-1-piperaziny) ethanesulfonic acid.
[b] HEPES previously was dissolved in 100 mL of 0.2 M-NaOH aqueous solution.
[a] Buffered at pH 7.4 at 36.5 °C with HEPES and 1.0 M-NaOH aqueous solution.

Several types of physiological fluids such as SBFs, artificial saliva and phosphate buffer solutions are used in electrochemical studies performed at body temperature (Table 1). In these biological media, PEO coatings have shown higher corrosion resistance than unmodified titanium alloy substrates [52–58]. The composition and, in particularly, the thickness of bioactive PEO coatings may vary greatly in different studies. Even in case of today's only commercial PEO-coated dental implant TiUnite® (Nobel Biocare), which contains about 5–8% of phosphorus, the thickness, reportedly, varies from ~2 to ~9 μm [59,60]. Due to the mechanism of PEO coatings formation, their composition will depend on the treatment time, and therefore, on the coating thickness. The fabrication of thicker coatings requires greater energy consumption, and consequently, is more costly.

In this study two types of PEO coatings on commercially pure titanium with different Ca/P ratios and two different thicknesses each, are being examined with the aim of underpinning the effect of coating composition, thickness and microstructure on the corrosion behavior and hydroxyapatite forming ability in SBF.

2. Experimental methods

2.1. Materials

Specimens of dimensions 30 × 20 × 0.5 mm were cut from commercially pure (c.p.) Grade I titanium foil (0.2 Fe, 0.18 O, 0.03 N, 0.015 H, and 0.18 C (max wt%)), degreased in isopropanol and rinsed in distilled water. Following subsequent pickling for ~20 s in a mixture containing 12 mL HF (40 wt%), 40 mL HNO_3 (70 wt%) and 48 mL H_2O at room temperature, the specimens were rinsed in distilled water, dried and masked with Lacquer 45 resin (McDermid plc.) to isolate a working area of 3 cm^2.

2.2. Surface treatment

PEO treatment was carried out for 90 and 600 s using a 2 kW regulated AC power supply (EAC-S2000, ET Systems electronic). A square waveform voltage signal was applied with a positive-to-negative pulse ratio of 490 V/60 V at 50 Hz frequency and initial ramp of 60 s to achieve the voltage

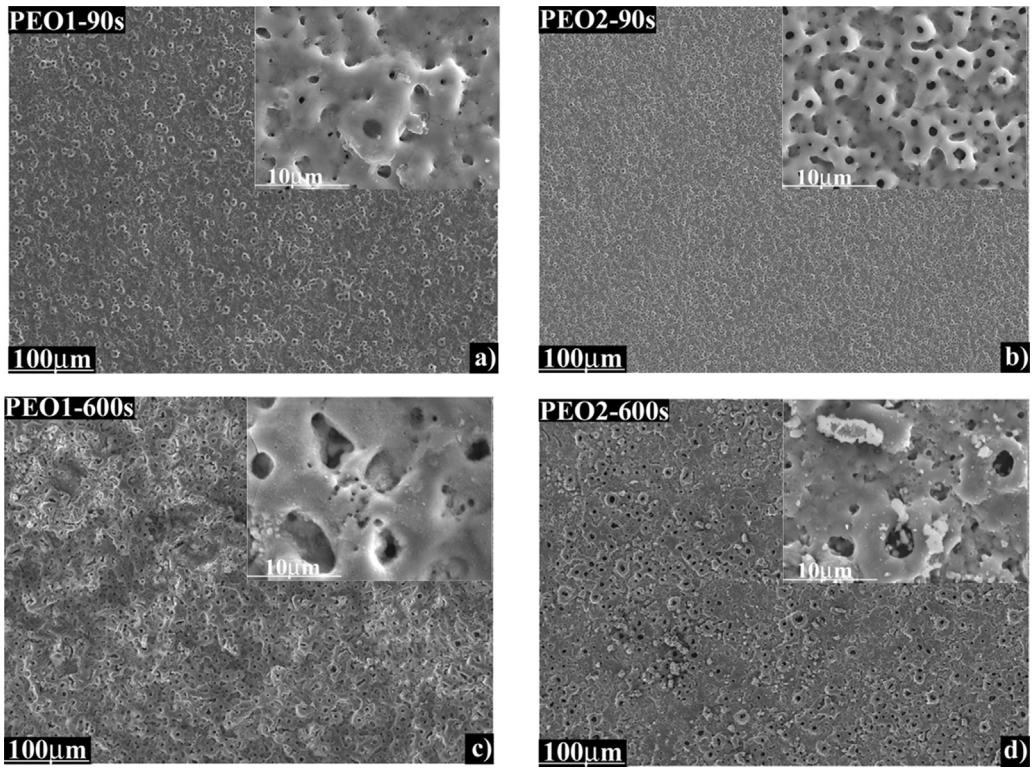

Fig. 1 – Plan view secondary electron images of the titanium substrate after PEO treatments; (a) PEO1-90 s, (b)PEO2-90 s, (c) PEO1-600 s, (d) PEO2-600 s.

amplitude. The root mean square (rms) current density limit was set at 400 mA cm^{-2}, while the voltage peak-to-peak value was maintained constant. The rms voltage and current responses were acquired electronically, with a sampling time of 0.1 s, employing a Keithley KUSB-3116 data acquisition card (16 bit, 500 kS s^{-1}) and Labview program (National Instruments). Instantaneous voltage and current values were monitored and recorded using a 2-channel Tektronix TDS 2012B oscilloscope at 100 MHz sampling rate.

PEO1 coating was generated in the electrolyte based on calcium acetate and sodium hexametaphosphate with ratio of Ca/P = 2; PEO2 coating was formed in calcium acetate and sodium dihydrogen phosphate solution with Ca/P = 5. Both electrolytes were suspensions with pH 7.0. The treatment was performed in a 1 L double-walled cell with re-circulating cooling system that maintained the temperature of the electrolyte at 20 °C. The cathode was made of AISI 316 stainless steel and had dimensions of 7.5 × 15 cm. After PEO, the specimens were rinsed in distilled water and dried in warm air.

2.3. *Surface characterization*

Coating thicknesses were measured by the eddy current method, using a Fischer ISOSCOPE FMP10 portable instrument, taking the average of ten measurements with a standard deviation of ~0.5 μm and later confirmed with cross-sectional scanning electron microscopy (SEM). Plan views and cross-sections of coatings were examined by SEM, using a JEOL JSM-6400 microscope equipped with Oxford Link energy dispersive X-ray (EDX) microanalysis hardware. EDX surface area analysis results are cited as an average of three measurements performed at different locations. Cross-sections were prepared by grinding through successive grades of silicon carbide paper, with final polishing to a 1 μm diamond finish. Phase composition was examined by X-ray diffraction (XRD), using a Philips X'Pert diffractometer (Cu $K\alpha = 1.54056$ Å) at a scanning speed of 0.01° per second for a scan range of 2θ from 10° to 80°. Surface hardness was measured on polished cross-sections applying a load of 0.05 kg for 15 s using an AKASHI MVK-E3 Vickers microhardness machine. The cited values are the average of ten measurements. Roughness parameter R_a (arithmetic average of the absolute profile deviations within the scanning path) was obtained using a Surtronic 25 roughness tester (Taylor Hobson) and TalyProfile software applying a Gaussian filter of 0.4 mm. The presented values are the average of 5 measurements performed over a distance of 4 mm. The pore population density and pore size of the coatings have been estimated using UTHSCSA Image Tool software.

2.4. *Immersion tests*

Coated and untreated substrates of c.p. Ti were exposed to a simulated body fluid solution (SBF, Table 2) as in [61] with a pH 7.4 for times up to 4 weeks. Each specimen was immersed in 25 mL of the solution, placed in a tightly-sealed container, and thermostated at 37 °C. Two specimens for each type of material were used for reproducibility.

2.5. *Electrochemical tests*

DC and AC electrochemical tests were carried out using an AUTOLAB PGSTAT30 (Eco Chemie) potentiostat in naturally

Table 3 – Surface EDX analysis of the material composition before immersion.

Material	Elements (at%)							
	O	P	Ca	Ti	Fe	Ca/P	Ca/Ti	P/Ti
Ti CP	–	–	–	99.7 ± 0.5	0.3 ± 0.1	–	–	–
PEO1-90 s	61.3 ± 7.5	2.4 ± 0.5	3.7 ± 1.3	32.6 ± 1.2	–	1.5	0.11	0.07
PEO2-90 s	59.9 ± 8.9	2.3 ± 0.5	4.6 ± 1.2	33.2 ± 1.2	–	2	0.13	0.07
PEO1-600 s	73.6 ± 8.9	6.5 ± 1.3	11.1 ± 2.7	8.5 ± 1.1	–	1.71	1.31	0.76
PEO2-600 s	66.1 ± 4.6	1.5 ± 0.3	6.0 ± 1.7	26.4 ± 4.1	–	4.00	0.22	0.06

aerated SBF solution at 37 °C. All measurements were reproduced at least twice. Potentials were measured with respect to a Ag/AgCl reference electrode. Solution concentration inside the reference electrode compartment was 3 M KCl, providing a potential of 0.210 V with respect to the standard hydrogen electrode. A platinum foil (~1 cm^2) was used as the auxiliary electrode. The specimens were polarized at a rate of 0.3 mV s^{-1} from −250 to +3500 mV relative to the OCP. Electrochemical impedance spectroscopy (EIS) or, AC measurements, were carried out applying a sinusoidal perturbation of 10 mV amplitude and a frequency sweep from 10^5 to 10^{-2} Hz. The frequency response was analyzed using ZView software, the goodness of fit of the simulated spectra corresponded to chi-squared (square of the standard deviation between the original data and the calculated spectrum) values <0.01. The errors for the individual parameters of the equivalent electrical circuits (such as *CPE* and *R*) were <5%.

2.6. *Ion release analysis*

The immersion test solutions were acidified with 200 μL of nitric acid (65 wt%) to dissolve precipitated titanium hydroxide. After filtering through a nylon filter with 22 μm pore size and 1:6 dilution in Millipore water, the samples were analyzed by inductively coupled plasma mass spectroscopy (ICP–MS) using an Agilent 7700 ICP–MS instrument equipped with concentric quartz nebulizer and Peltier-cooled nebulizing camera. The instrument was operated in standard mode, without using the reaction cell.

Argon was used as plasma maintaining carrier gas. ICP–MS operating conditions were as follows: forward power 1550 W, argon flow 0.99 L min^{-1}, nebulizer pump 0.3 rps.

Three titanium isotopes were measured simultaneously (^{47}Ti, ^{48}Ti and ^{49}Ti). Calibrations based on ^{47}Ti were made using both deionized water and 1:6 diluted SBF-blank solution in the range from 0 to 50 μg L^{-1}. The calibration curve was corrected with respect to a background level of Ti detected in blank SBF (22.7 ppb). The other two isotopes reflected to a greater (^{48}Ti) or lesser (^{49}Ti) extent the effects of the SBF-matrix. The results are cited as an average of two measurements with the errors representing the deviation of the maximum and minimum from the mean.

3. Results and discussion

3.1. *Coating morphology and microstructure*

Fig. 1 shows the surface morphologies of PEO1 and PEO2 coatings. The higher magnification images of the surfaces (insets) reveal submicron-size morphological differences in the superficial deposits originating from the electrolytes. Local EDX analysis, conducted in different areas of the coating surface, revealed that the respective surface compositions of each coating were fairly uniform. The average Ca/P surface ratio was 1.5 and 1.7 for PEO1-90 s and -600 s, respectively, which is close to stoichiometric hydroxyapatite (HA). PEO2-90 s contained similar absolute amounts of Ca and P to PEO1-90 s with an average Ca/P of ~2, whereas PEO2-600 s showed ~4 and ~2 times lower amount of Ca and P, respectively, compared with PEO1-600 s, and its average Ca/P ratio was ~4 (Table 3).

As shown in Table 4, after 600 s of PEO treatment, both coatings exhibited similar microhardness values. PEO1 had slightly greater roughness than PEO2, increasing this difference for a longer PEO treatment time. The lower limit of pore size is similar for all the coatings. The pores arise at the sites of the discharges channels due to the gas evolution through the molten oxide material during the PEO process; the upper limit of the pore size increases with treatment time and is the largest (~13 μm) for PEO1. The pore population density did not exhibit a clear dependency on the treatment time.

The cross sections of the coatings prepared at the different conditions are shown in Fig. 2. The examination of the backscattered scanning electron micrographs revealed relatively uniform coatings comprising an outer porous layer and an approximately 0.5–1 μm-thick barrier layer adjacent to the substrate (Fig. 2). For 90 s of treatment, PEO1 and PEO2 coatings were ~6 μm- and ~4 μm-thick, respectively, revealing voids and cavities typical of the coating process. The thickness of both coatings significantly increased (to ~16–19 μm) when

Table 4 – Surface characteristics of the developed coatings.

	PEO1-90 s	PEO2-90 s	PEO1-600 s	PEO2-600 s
Microhardness (HV)	–	–	276.5 ± 5.2	270.1 ± 4.2
Roughness (μm)	R_a = 0.91 ± 0.18 R_z = 5.69 ± 1.0	R_a = 0.58 ± 0.11 R_z = 3.55 ± 0.71	R_a = 1.63 ± 0.32 R_z = 9.08 ± 1.81	R_a = 1.28 ± 0.26 R_z = 6.5 ± 1.3
Pore size (μm)	0.4–3	0.4–2	0.4–12.7	0.4–6.2
Pore population density (pore mm^{-2})	~45,000	~100,000	~50,000	~40,000

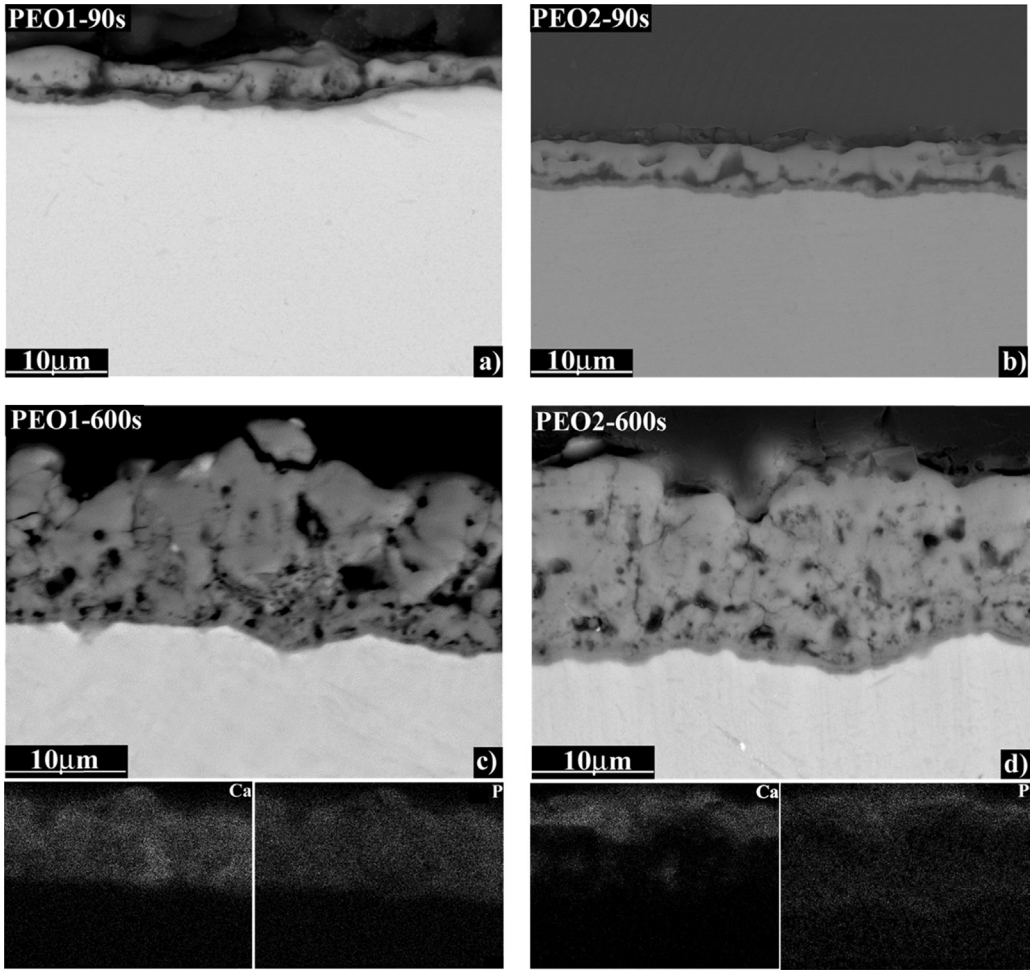

Fig. 2 – Backscattered electron images of the coatings cross sections(a) PEO1-90 s, (b) PEO2-90 s, (c) PEO1-600 s and respective X-ray elemental maps, (d) PEO2-600 s and respective X-ray elemental maps.

the PEO time was increased to 600 s. X-ray elemental mapping of PEO1 coating revealed that Ca and P species were homogeneously distributed throughout the coating thickness, whereas for PEO2 coating, these elements were mostly located in the external part.

XRD surface analysis revealed the presence of anatase and rutile in all of the studied coatings (Fig. 3). Additionally, PEO1-600 s comprised apatite, $Ca_3(PO_4)_2$, and amorphous material, manifested as a hump between ~25 and ~35 2θ. No crystalline Ca and/or P containing phases were detected for the other coated materials. PEO2-600 s also contained some amorphous material, although to a much lesser extent. According to the corresponding peak intensities, PEO2-600 s contained more rutile than anatase, whereas the reverse was true for PEO1-600 s. PEO1-90 s and PEO2-90 s were completely crystalline with fairly similar phase composition.

After immersion in SBF solution for 7 d, only Ti CP and the PEO2-600 s coating were covered by the newly formed layer of HA (Fig. 4), confirmed by X-ray analysis (Fig. 4(c)) with an apparent thickness of few micrometers. The concentrations of both Ca and P in PEO2-600 s increased after immersion in SBF solution to 23.5 and 14.0 at%, respectively. Interestingly, after 28 days of immersion most of the surface of both PEO1 coatings, was covered by an amorphous film (confirmed by XRD, not shown) (Fig. 5) with much increased content of Ca (10.9–12.1 at%) and P (6.1–6.9 at%), compared with the coating composition before immersion. The ~1.8 Ca/P ratio of this deposit suggests that it could be amorphous hydroxyapatite [62,63], although more analysis are needed to confirm this. Previously we have reported that PEO2-600 s induced greater osteoblast cell proliferation rate than PEO1-600 s, although both of the coatings were found to increase the bioactivity of titanium [20].

3.2. *OCP measurements*

The variation of open circuit potentials (OCP) for all the studied materials in SBF solution at 37 °C for a period of 1 h are shown in Fig. 6. All the PEO coatings reached at the early stage of immersion a steady OCP value 400–500 mV higher than that of Ti CP, whose OCP gradually increased during the test duration up to $-320\,mV_{Ag/AgCl}$, suggesting the formation of a protective and stable oxide film on the surface.

3.3. *DC polarization response*

DC polarization curves of tested materials in m-SBF solution were highly reproducible. The Ti CP showed an E_{corr} of about $-200\,mV_{Ag/AgCl}$ after 4 weeks of immersion in SBF solution.

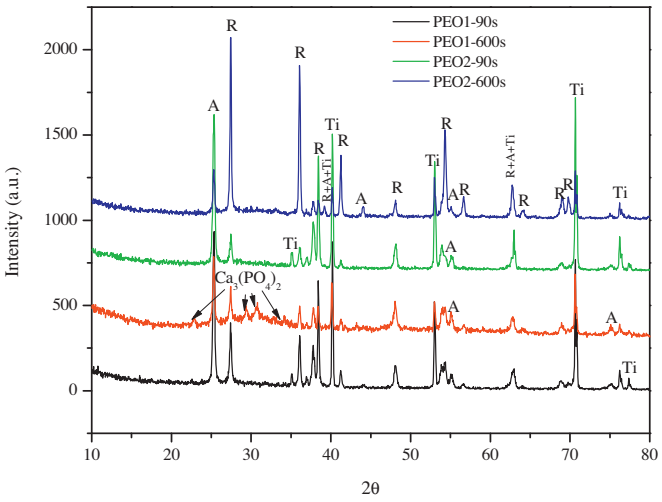

Fig. 3 – X-ray diffraction patterns of the PEO-coated Ti. A—anatase; R—rutile.

The anodic branch showed an active corrosion region, typically associated with the formation of soluble Ti^{3+} ions [64], followed by a passive region, corresponding to the formation of a passive TiO_2 film, with current densities of ~0.7 μA cm^{-2}. This passive region extended from ~600 to ~1400 $mV_{Ag/AgCl}$ and was followed by an increase in current density due to oxygen evolution on the surface of the oxide (Fig. 7, Table 5).

E_{corr} values of PEO coatings were by ~75 mV (PEO1-90 s), ~45 mV (PEO1-600 s), ~40 mV (PEO2-90 s) and ~11 mV (PEO2-90 s) nobler than those of Ti CP. No Tafel (active dissolution)

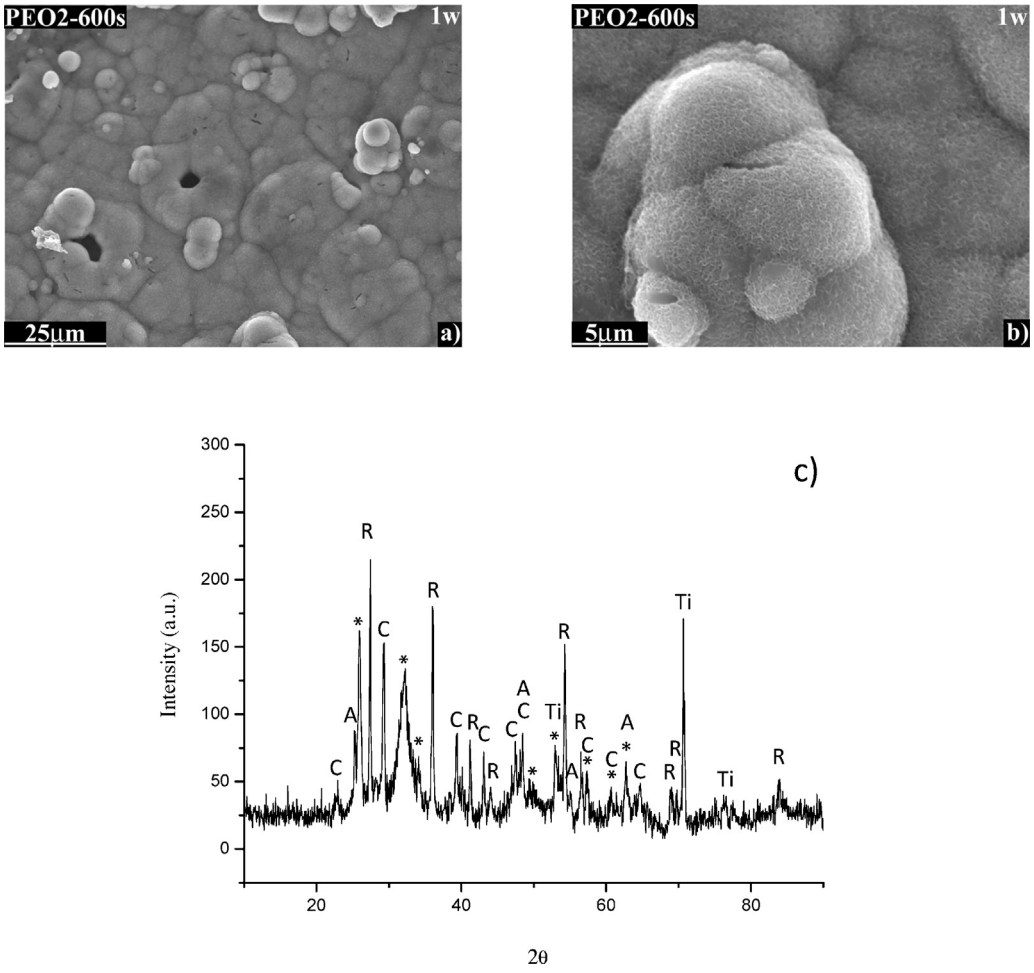

Fig. 4 – PEO2-600 s coating after 1 week of immersion in SBF: (a and b) surface morphology and (c) X-ray diffraction patterns. A—anatase; R—rutile; +—hydroxyapatite; C—$CaCO_3$.

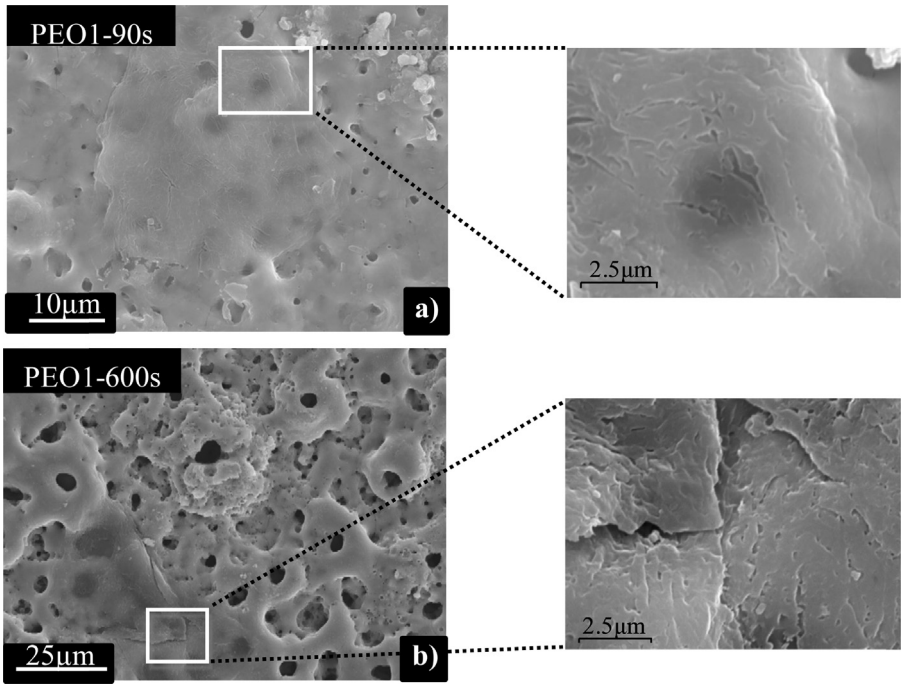

Fig. 5 – Secondary electron images of the surface morphology of (a) PEO1-90 s and (b) PEO1-600 s coatings after 4 weeks of immersion in SBF.

region was present and the passive regions extended from the E_{corr} values to ~2500 $mV_{Ag/AgCl}$. The passive current densities for PEO1 (90 and 600 s) and PEO2 (90 and 600 s) were, respectively, ~30 and ~10 times lower than those for Ti CP, indicating their higher electrochemical stability. PEO1-90 s exhibited the lowest j_{pas} of all the coated materials, indicating its greatest passivity, *i.e.* the slowest ion exchange at the metal/coating interface.

3.4. *Ion liberation*

Fig. 8 shows Ti^{4+} ion release of studied materials following immersion in SBF for 1 and 4 weeks. Ion release for Ti CP increased linearly with time, *i.e.* Ti^{4+} concentration was 4 times higher after 4 weeks of immersion. The amounts of oxidized titanium calculated using Faraday's law and i_{corr} values obtained by DC polarization were 1.74 and 1.92 $\mu g\,cm^{-2}$ for 1 and 4 weeks of immersion, respectively. As can be seen in Fig. 8, the actual amount of Ti ions released into the media was ~1% and ~25% of the calculated values, respectively. This indicated that the passivation capacity of Ti CP decreased for protracted times of immersion, *i.e.* 25% of generated Ti^{4+} ions are being ejected into the solution instead of being built into the TiO_2 film.

All four PEO-coated materials exhibited similar or slightly smaller Ti^{4+} ion release than Ti CP after 1 week of

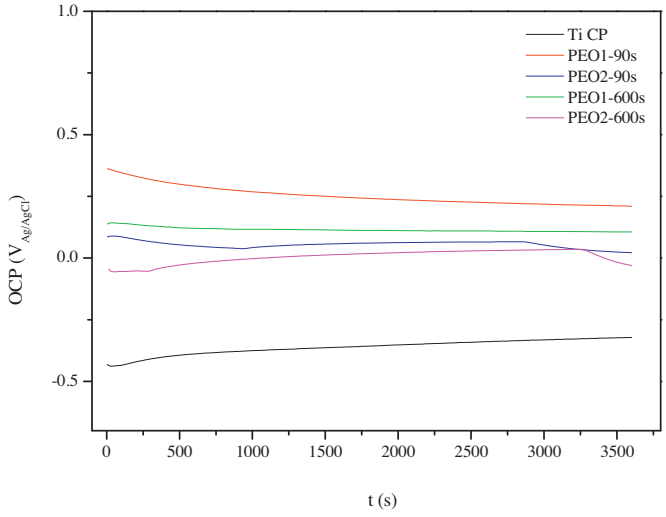

Fig. 6 – Variation of open circuit potentials (OCP) for all the studied materials immersed in SBF solution at 37 °C for 1 h.

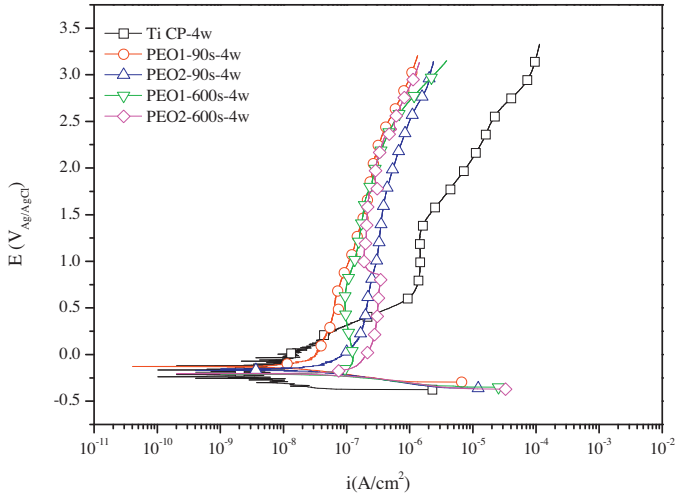

Fig. 7 – DC polarization curves for all the studied materials immersed in SBF solution at 37 °C for 4 weeks.

immersion in SBF, and 2 to 4 times lower Ti^{4+} ion release after 4 weeks (Fig. 8). A few inferences can be made regarding the influence of the coating thickness and composition on the mechanism and level of the metal ion release:

(i) After 1 week of immersion the materials with both thick and thin PEO1 type coatings, showed ~23–29% higher Ti^{4+} release than the uncoated substrate, which suggests chemical dissolution of the coating material itself. PEO2 coated materials, on the contrary, released ~25–46% less Ti^{4+} than the uncoated substrate, suggesting that these coatings are chemically more stable and present a barrier for the electrochemical dissolution of the substrate.

(ii) The increase of Ti^{4+} release from week one to week four was negligible in both thick and thin PEO1 coatings and in thin PEO2. However, PEO2-600 s exhibited an almost 4 times increase of the ion release over 4 weeks.

(iii) Comparing the stability of the materials with thin coatings over 4 weeks of immersion, PEO2-90 s revealed ~40% lower titanium ion release than PEO1-90 s.

(iv) Comparing the stability of the materials with thick coatings, PEO2-600 s released ~50% more Ti^{4+} than PEO1-600 s.

(v) After four weeks of immersion, the lowest Ti^{4+} release was observed from titanium coated by PEO2-90 s.

The highest level of Ti^{4+} release into SBF detected from PEO coated material (PEO2-600 s) over the period of 4 weeks corresponds to 30 ppb; this value is far below the level of 5 ppm, reported as cytotoxic [65]. Considering that the tested sample area of 3 cm^2 is similar to the area of an average dental

Table 5 – Parameters of the polarization curves.

Material	Time	E_{corr} ($V_{Ag/AgCl}$)	i_{corr} (A/cm^2)	i_{pas} (A/cm^2)
Ti CP	1 h	−0.248	5.42×10^{-8}	1.32×10^{-6}
PEO1-90 s		0.123	–	1.61×10^{-8}
PEO2-90 s		0.042	–	1.97×10^{-8}
PEO1-600 s		−0.012	–	1.12×10^{-7}
PEO2-600 s		−0.123	–	5.92×10^{-8}
Ti CP	1 d	−0.106	4.62×10^{-9}	1.45×10^{-6}
PEO1-90 s		−0.056	–	3.37×10^{-8}
PEO2-90 s		0.023	–	1.58×10^{-8}
PEO1-600 s		−0.073	–	6.32×10^{-8}
PEO2-600 s		−0.062	–	7.25×10^{-8}
Ti CP	7 d	−0.152	5.8×10^{-9}	9.31×10^{-7}
PEO1-90 s		−0.059	–	4.31×10^{-8}
PEO2-90 s		−0.113	–	2.11×10^{-7}
PEO1-600 s		−0.075	–	1.93×10^{-7}
PEO2-600 s		−0.143	–	9.38×10^{-8}
Ti CP	28 d	−0.200	6.46×10^{-9}	6.49×10^{-6}
PEO1-90 s		−0.125	–	7.12×10^{-8}
PEO2-90 s		−0.160	–	2.03×10^{-7}
PEO1-600 s		−0.185	–	1.68×10^{-7}
PEO2-600 s		−0.189	–	3.22×10^{-7}

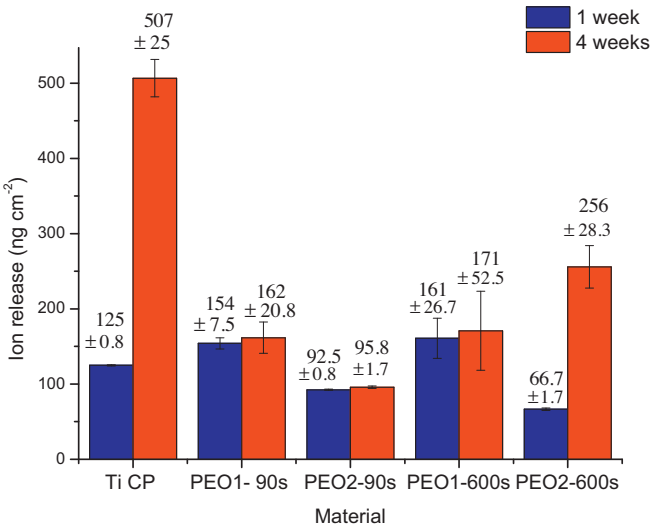

Fig. 8 – Results of Ti^{4+} ion release for all the studied materials immersed in SBF solution at 37 °C for 1 and 4 weeks.

implant (2 cm^2), it would take about 14 years to reach that concentration, assuming a linear rate of ion release.

3.5. *EIS response*

Next, electrical characteristics of the coatings will be considered in order to verify the corrosion behavior observed *in-vitro* and to try to underpin the mechanism of the PEO coatings degradation.

Fig. 9 shows Nyquist (a) and Bode (b) diagrams of EIS response of Ti CP in SBF measured for up to four weeks of immersion. Insets in Fig. 9(b) show equivalent circuits used for simulation of the electrical parameters of the material. A Randles circuit comprising constant phase element (CPE_b) and resistance (R_b), describes the capacitive and resistive behavior, respectively, of the thin, naturally formed barrier TiO_2 film on the surface of Ti CP for 1 h of immersion. Capacitive behavior is related to the dielectric nature of TiO_2 and the presence of a double electric layer on the metal/electrolyte interface. Constant phase element reflects the heterogeneous nature of the oxide film, which behaves as a non-ideal capacitor.

The impedance of a *CPE* is calculated as $Z = 1/[CPE(j\omega)^n]$; where ω is radial frequency, n is the exponential factor ($-1 \le n \le 1$) and $j = \sqrt{-1}$ is the imaginary number. *CPE* corresponds to a numerical value of admittance of the system, 1/Z, at $\omega = 1$ rad s^{-1}. With $n = 1$, constant phase element becomes an ideal capacitor. Capacitance depends on the thickness of the oxide film. The capacitance value of 18.4 μF cm^{-2} derived from the CPE_b of 22.4 μS s^n cm^{-2} (Table 6) can be used to calculate the oxide film thickness [55] and corresponds to 2 nm-thick oxide film.

After 1 day of immersion a second time constant appears (Fig. 9(b)) possibly due to the precipitation of hydroxiapatite (HA) layer on the surface of titanium, which presents and additional resistance; the HA layer is simulated with $CPE_{ads}R_{ads}$ element. The HA layer thickens with time, as can be seen from increase of its resistance, R_{ads}, and capacitive behavior,

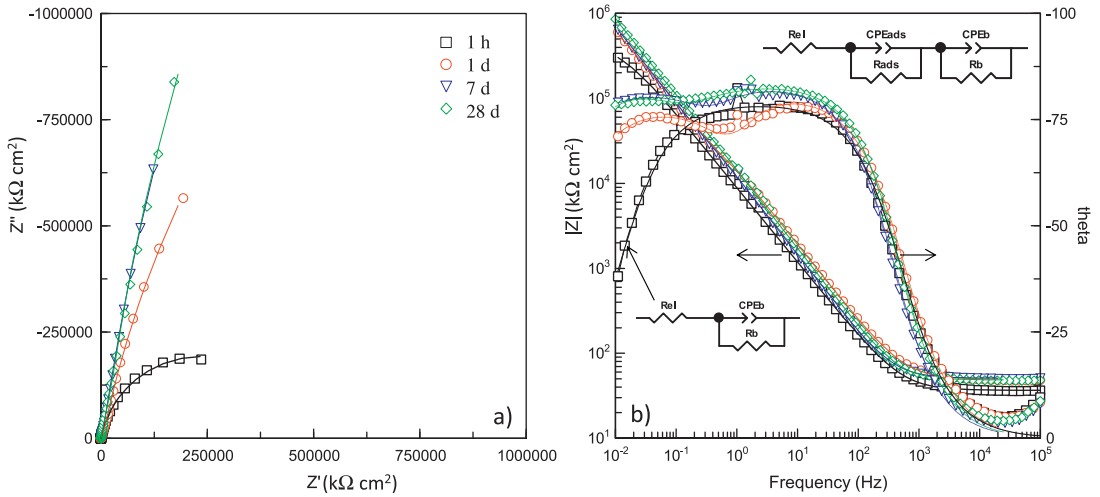

Fig. 9 – Nyquist (a) and Bode (b) diagrams of EIS response of untreated titanium in SBF measured up to 4weeks.

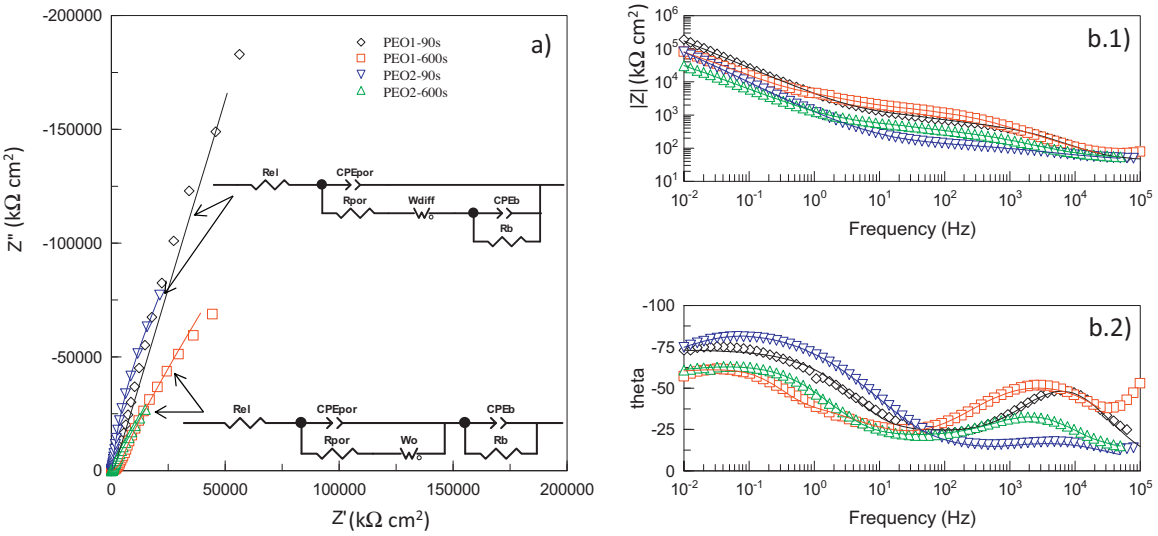

Fig. 10 – Nyquist (a) and Bode (b) diagrams of EIS response of PEO coatings in SBF measured up to 4weeks.

CPE_{ads} (Table 5); this, in turn, increases the impedance modulus $|Z|$ of titanium at low frequencies as can be seen in Fig. 9(b), which indicates the improved electrochemical stability of the material.

For all times of immersion the impedance response for both types of PEO coatings (thin and thick) showed two time constants (at ~5 kHz and ~100 mHz), corresponding, respectively to the impedance of the porous and barrier parts of the coating, (Fig. 10) which is typical for PEO coatings on titanium in NaCl solutions [10,27,66,67]. Good fits of the experimental data were obtained using a "nested" equivalent electrical circuit (Fig. 10(a), inset), where CPE_{por} and CPE_b correspond to the capacitive behavior of the porous and barrier parts of the PEO coating, respectively; R_{por} is a resistance of the electrolyte filling the pores and R_b is the resistance of the barrier part. A finite length Warburg diffusion element with open circuit terminus, W_o, included in series with the resistance of the porous part, R_{por}, accounts for mass-transfer processes inside the outer porous part of the PEO coating [68]. Mathematical expressions for the impedance of the above parameters are given elsewhere [68].

The simulated parameters of the equivalent circuit are summarized in Table 7. Some notable correlation between the variation of the electrical parameters of the coatings with time and Ti^{4+} ion release, discussed above, can be discerned.

Regarding the previously described fact of greater ion release from the PEO1-90 s material in 1st week of immersion than from the uncoated substrate: a decrease of the resistance of the porous part of the coating, R_{por}, by an order of magnitude over the course of 28 days, while the resistance of its barrier part, R_b, steadily increased (Table 7) corroborates the suggestion that a chemical degradation of the coating occurs to a certain degree. Further, R_{por} of PEO2-90 s is much lower (approximately equal to the resistance of the SBF solution) than that of PEO1-90 s and it remains practically unchanged over time, meaning that the porous part of PEO2-90 s is fully permeable by the electrolyte, but the degradation of coating material is negligible. The latter correlates well with the observed increase of the diffusion resistance $W_o - R$ (from ~0.4 to ~10 kΩ cm^2). It was suggested that finite diffusion W_o element describes not only diffusion of the species through the open pores, but also diffusion of the vacancies through the oxide [68], in which case the observed increase of $W_o - R$ and especially of $W_o - T$ (the life time of the diffusion specie) suggests decrease of the number of vacancies, *i.e.* that the stoichiometry of the oxide gets closer to pure TiO_2.

Similarly, a large drop in R_{por} of PEO2-600 s from 2.24 kΩ cm^2 for 7 day to ~0.43 kΩ cm^2 for 28 days correlates with the observed increase of Ti^{4+} released into SBF over that period. Previously we reported that PEO2-600 s also exhibits a considerable release of Ca and P [55]; also, PEO2-600 s exhibited greater bioactivity with respect to proliferation of mice osteoblast cells *in-vitro* than PEO1-600 s [20]. We have discussed in [20] that overstoichiometric ratio of Ca/P (with respect to stoichiometry of hydroxyapatite) determines the

Table 6 – Simulated parameters of the EIS equivalent circuits obtained for Ti CP up to 4 weeks of immersion in SBF.

Immersion time	CPE_{ads} (μS s^n cm^{-2})	n	R_{ads} (kΩ cm^2)	CPE_b (μS s^n cm^{-2})	n	R_b (MΩ cm^2)
1 h	–	–	–	22.4	0.88	0.48
1 d	40.6	1	3.68	17.3	0.87	4.87
7 d	105.0	1	3.62	17.6	0.91	12.25
28 d	79.2	0.9	14.14	14.92	0.93	10.04

Table 7 – Simulated parameters of the EIS equivalent circuits obtained for PEO-coated titanium up to 4 weeks of immersion in SBF.

Material	Time	$CPE_b - T$ ($\mu S\, s^n\, cm^{-2}$)	n	R_b ($k\Omega\, cm^2$)	$W_o - R$ ($k\Omega\, cm^2$)	$W_o - T$ (s)	n	$CPE_{por} - T$ ($\mu S\, s^n\, cm^{-2}$)	n	R_{por} ($k\Omega\, cm^2$)
PEO1-90 s	1 h	271.5	0.99	1.02	7.34	0.33	0.43	2.2	0.81	3.75
	1 d	300.5	0.99	93.75	4.86	0.48	0.43	2.8	0.79	4.80
	7 d	138.9	1.0	509.42	5.52	0.64	0.35	1.3	0.82	1.69
	14 d	88.8	0.97	1166.70	7.34	1.76	0.32	0.8	0.86	1.36
	28 d	62.4	0.89	1700.90	6.85	8.86	0.36	1.0	0.84	0.44
PEO2-90 s	1 h	6.6	0.75	19.91	0.41	0.02	0.50	6.4	0.53	0.07
	1 d	0.2	0.98	11.65	6.86	0.47	0.51	20.3	0.62	0.08
	7 d	238.4	0.96	119.10	3.28	0.5	0.43	8.6	0.76	0.17
	14 d	137.7	1.0	965.22	10.46	517.9	0.42	21.3	0.70	0.08
	28 d	159.1	0.99	501.00	8.22	107.8	0.46	15.2	0.70	0.06
PEO1-600 s	1 h	312.6	0.87	21.70	14.26	1.37	0.40	5.0	0.73	2.67
	1 d	450.0	0.9	21.22	9.65	1.40	0.40	3.5	0.75	3.68
	7 d	454.2	0.80	25.35	9.93	0.60	0.37	2.4	0.79	1.58
	28 d	179.3	0.82	88.40	7.46	1.87	0.40	2.4	0.77	1.08
PEO2-600 s	1 h	538.7	0.83	19.28	7.92	1.81	0.40	14.1	0.67	1.81
	1 d	951.1	0.99	18.42	9.97	3.63	0.36	14.9	0.67	1.08
	7 d	1412.8	0.99	20.78	13.67	2.62	0.37	11.4	0.68	2.24
	28 d	470.5	0.99	32.31	13.14	14.02	0.59	26.7	0.61	0.43

enhanced bioactivity of PEO2-600 s compared with PEO1-600 s. If Ca and P in PEO2-600 s are doping the lattices of anatase and rutile, their release will proceed relatively easy, which in turn will create defects (vacancies) in TiO_2, affecting its chemical stability.

4. Conclusions

PEO coatings impeded Ti ion release into the SBF over the period of 4 weeks. The detected metal ion release is attributed mostly to chemical dissolution of the coatings, which occurs at initial stages of immersion. The long term stability was greater for thin PEO coating with overstoichiometric Ca/P ratio of 2.0, which exhibited ~95 ng cm^{-2} of Ti^{4+} ions release over 4 weeks. The stability of PEO1 coatings with Ca/P ratio of 1.5 and 1.7 was practically independent of the coating thickness over the period of 4 weeks. The lowest stability, *i.e.* the highest metal ion release was observed for the thick PEO coating with Ca/P ratio of 4.0. On the other hand, this coating exhibited capacity to induce the precipitation of a thick uniform hydroxyapatite layer over the short period of 1 week, whereas other investigated coatings did not. Further studies *in-vitro* using cell cultures are required in order to further elucidate the bioactivity of thinner PEO coatings; in case found adequate, thin PEO coatings would present economically more viable and more corrosion resistant option to insure long-term service life of an implant.

REFERENCES

[1] Browne M, Gregson PJ. Surface modification of titanium alloy implants. Biomaterials 1994;15:894–8.

[2] Ibris N, MirzaRosca JC. EIS study of Ti and its alloys in biological media. Journal of Electroanalytical Chemistry 2002;526:53–62.

[3] Narayanan R, Seshadri SK. Point defect model and corrosion of anodic oxide coatings on Ti–6Al–4V. Corrosion Science 2008;50:1521–9.

[4] Han Y, Chen D, Sun J, Zhang Y, Xu K. UV-enhanced bioactivity and cell response of micro-arc oxidized titania coatings. Acta Biomaterialia 2008;4:1518–29.

[5] Larsson C, Thomsen P, Lausma J, Rodahl M, Kasemo B, Ericson. Bone response to surface modified titanium implants: studies on electropolished implants with different oxide thicknesses and morphology. Biomaterials 1994;15:1062–74.

[6] Cochran DL, Schenk RK, Lussi A, Higginbot FL, Buser D. Bone response to loaded and unloaded titanium implants with a sandblasted and acid etched surface: a histometric study in the canine mandible. Journal of Biomedical Materials Research Part A 1998;40:1–11.

[7] Blind O, Klein L, Dailey B, Jordan L. Characterization of hydroxyapatite films obtained by pulsed-laser deposition on Ti and Ti–6Al–4V substrates. Dental Materials 2005;21:1017–24.

[8] Dey T, Roy P, Fabry B, Schmuki P. Anodic mesoporous TiO_2 layer on Ti for enhanced formation of biomimetic hydroxyapatite. Acta Biomaterialia 2011;7:1873–9.

[9] Giordano C, Chiesa R, Sandrini E, Cigada A, Giavaresi G, Fini M, Giardino R. Biological characterization of a novel multiphase anodic spark deposition coating to enhance implant osteointegration. Journal of Materials Science Materials in Medicine 2005;16:1221–9.

[10] Krupa D, Baszkiewicz J, Zdunek J, Smolik J, Slomka Z, Sobczak JW. Characterization of the surface layers formed on titanium by plasma electrolytic oxidation. Surface and Coatings Technology 2010;205:1743–9.

[11] Sul YT, Johansson C, Byon E, Albrektsson T. The bone response of oxidized bioactive and non-bioactive titanium implants. Biomaterials 2005;26:6720–30.

[12] Kweh SWK, Khor KA, Cheang P. An in vitro investigation of plasma sprayed hydroxyapatite (HA) coatings produced with flame-spheroidized feedstock. Biomaterials 2002;23:775–85.

[13] HabibovicP, Barrere F, Blitterswijk CA, Groot K, Layrolle P. Biomimetic hydroxyapatite coating on metal implants. Journal of American Ceramic Society 2002;85:517–22.

[14] Lee SY, Piao CM, Koak JY, Kim SK, Kim YS, Ku Y, Rhyu IC, Han CH, Heo SJ. A 3-year prospective radiographic evaluation of marginal bone level around different implant systems. Journal of Oral Rehabilitation 2010;37:538–44.

[15] Friberg B, Jemt T. Clinical experience of TiUnite® implants: a 5-year cross-sectional, retrospective follow-up study.

Clinical Implant Dentistry and Related Research 2010;12:95–103.
[16] Yerokhin AL, Nie X, Leyland A, Matthews A. Characterisation of oxide films produced by plasma electrolytic oxidation of a Ti–6Al–4V alloy. Surface and Coatings Technology 2000;130:195–206.
[17] Curran JA, Clyne TW. The thermal conductivity of plasma electrolytic oxide coatings on aluminium and magnesium. Surface and Coatings Technology 2005;199:177–83.
[18] Suh JY, Janga BC, Zhu X, Ong JL, Kim KH. Effect of hydrothermally treated anodic oxide films on osteoblast attachment and proliferation. Biomaterials 2003;24:347–55.
[19] Son WW, Zhu X, Shin HI, Ong JL, Kim KH. In vivo histological response to anodized and anodized/hydrothermally treated titanium implants. Journal of Biomedical Materials Research Part B: Applied Biomaterials 2003;66:520–5.
[20] Mohedano M, Guzman R, Arrabal R, LópezLacomba JL, Matykina E. Bioactive plasma electrolytic oxidation coatings—the role of the composition, microstructure and electrochemical stability. Journal of Biomedical Materials Research Part B: Applied Biomaterials 2013. DOI: 10.1002/jbm.b.32974.
[21] Chen JZ, Shi YL, Wang L, Yan FY, Zhang FQ. Preparation and properties of hydroxyapatite-containing titania coating by micro-arc oxidation. Materials Letters 2006;60:2538–43.
[22] Huang P, Xu KW, Han Y. Preparation and apatite layer formation of plasma electrolytic oxidation film on titanium for biomedical application. Materials Letters 2005;59:185–9.
[23] Kim MS, Ryu JJ, Sung YM. One-step approach for nano-crystalline hydroxyapatite coating on titanium via micro-arc oxidation. Electrochemistry Communications 2007;9:1886–91.
[24] Montazeri M, Dehghanian C, Shokouhfar M, Baradaran A. Investigation of the voltage and time effects on the formation of hydroxyapatite-containing titania prepared by plasma electrolytic oxidation on Ti–6Al–4V alloy and its corrosion behavior. Applied Surface Science 2011;257:7268–75.
[25] Nie X, Leyland A, Matthews A. Deposition of layered bioceramic hydroxyapatite/TiO_2 coatings on titanium alloys using a hybrid technique of micro-arc oxidation and electrophoresis. Surface and Coatings Technology 2000:125–407.
[26] Ni JH, Shi YL, Yan FY, Chen JZ, Wang L. Preparation of hydroxyapatite-containing titania coating on titanium substrate by micro-arc oxidation. Materials Research Bulletin 2008;43:45–53.
[27] Shi X, Xu L, Wang Q. Porous TiO_2 film prepared by micro-arc oxidation and its electrochemical behaviors in Hank's solution. Surface and Coatings Technology 2010;205:1730–5.
[28] Song W, Jun Y, Han Y, Hong S. Biomimetic apatite coatings on micro-arc oxidized titania. Biomaterials 2004;25:3341–9.
[29] Wang E, Nan K, Chen X, Ning C, Wang Z, Zhao N. Characterization of bioactive ceramic coatings prepared on titanium implants by micro-arc oxidation. Rare Metals 2006;25:84–9.
[30] Yang X, Yu Sirong, Li Wen. Preparation of bioceramic films containing hydroxyapatites on Ti–6Al–4V alloy surfaces by the micro-arc oxidation technique. Materials Research Bulletin 2009;44:947–9.
[31] Steinemann SG. Corrosion of surgical implants—*in vivo* and *in vitro* tests. In: Winter GD, Leray JL, Groot K, editors. Evaluation of biomaterials—advances in biomaterials. Chichester: Wiley; 1980. p. 1–34.
[32] McLachlan C, Farnell B, Galin H. Aluminum in human brain disease. In: Sarkar B, editor. Biological aspects of metals and metal-related diseases. New York, NY: Raven Press; 1983. p. 209–18.
[33] Cvijovic-Alagic I, Cvijovic Z, Mitrovic S, Panic V, Rakin M. Wear and corrosion behaviour of Ti–13Nb–13Zr and Ti–6Al–4V alloys in simulated physiological solution. Corrosion Science 2011;53:796–808.
[34] Callen BW, Sodhi RN, Griffiths K. Examination of clinical surface preparations on titanium and Ti–6Al–4V by X-ray photoelectron spectroscopy and nuclear reaction analysis. Progress in Surface Science 1995;50:269–79.
[35] French HG, Cook SD, Haddad RJ. Correlation of tissue reaction to corrosion in osteosynthetic devices. Journal of Biomedical Materials Research 1984;18:817–28.
[36] Browne M, Gregson PJ. Effect of mechanical surface pretreatment on metal ion release. Biomaterials 2000;21:385–92.
[37] Evans EJ. Cell damage in vitro following direct contact with fine particles of titanium, titanium alloy and cobalt–chrome–molybdenum alloy. Biomaterials 1994;15:713–7.
[38] Alves VA, Reis RQ, Santos ICB, Souza DG, Gonçalves T, Pereira-da-Silva MA, Rossi A, da Silva LA. In situ impedance spectroscopy study of the electrochemical corrosion of Ti and Ti–6Al–4V in simulated body fluid at 25 and 37 °C. Corrosion Science 2009;51:2473–82.
[39] Guo WY, Sun J, Wu JS. Electrochemical and XPS studies of corrosion behavior of Ti–23Nb–0.7Ta–2Zr–O alloy in Ringer's solution. Materials Chemistry and Physics 2009;113:816–20.
[40] Metikoss-Hukovic M, Kwokal A, Piljac J. The influence of niobium and vanadium on passivity of titanium-based implants in physiological solution. Biomaterials 2003;24:3765–75.
[41] Luiz de Assis S, Wolynec S, Costa I. Corrosion characterization of titanium alloys by electrochemical techniques. Electrochimica Acta 2006;51:1815–9.
[42] Alves APR, Santana FA, Rosa LAA, Cursino SA, Codaro EN. A study on corrosion resistance of the Ti–10Mo experimental alloy after different processing methods. Materials Science and Engineering C 2004;24:693–6.
[43] Kumar S, Sankara Narayanan TSN. Electrochemical characterization of β-Ti alloy in Ringer's solution for implant application. Journal of Alloys and Compounds 2009;479:699–703.
[44] Fekry AM, Rabab M, El-Sherif. Electrochemical corrosion behaviour of magnesium and titanium alloys in simulated body fluid. Electrochimica Acta 2009;54:7280–5.
[45] Burstein GT, Liu C, Souto RM. The effect of temperature on the nucleation of corrosion pits on titanium in Ringer's physiological solution. Biomaterials 2005;26:245–56.
[46] Vieira AC, Ribeiro AR, Rocha LA, Celis JP. Influence of pH and corrosion inhibitor on the tribocorrosion of titanium in artificial saliva. Wear 2006;261:994–1001.
[47] Chung C, Kim H, Jeong Y, Son M, Jeong Y, Choe H. Electrochemical behavior of dental implant system before and after clinical use. Transactions of Nonferrous Metals Society of China 2009;19:846–51.
[48] Mabilleau G, Bourdon S, Joly-Guillou ML, Filmon R, Basle MF, Chappard D. Influence of fluoride, hydrogen peroxide and lactic acid on the corrosion resistance of commercially pure titanium. Acta Biomaterialia 2006;2:121–9.
[49] Ummethala R, Despang F, Gelinsky M, Basu B. In vitro corrosion and mineralization of novel Ti–Si–C alloy. Electrochimica Acta 2011;56:3809–20.
[50] Xie FX, He XB, Cao SL, Lu X, Qu XH. Structural characterization and electrochemical behavior of a laser-sintered porous Ti–10Mo alloy. Corrosion Science 2013;67:217–24.
[51] Pohrelyuk IM, Fedirko VM, Tkachuk OV, Proskurnyak RV. Corrosion resistance of Ti–6Al–4V alloy with nitride coatings in Ringer's solution. Corrosion Science 2013;66:392–8.

[52] Simka W. Preliminary investigations on the anodic oxidation of Ti–13Nb–13Zr alloy in a solution containing calcium and phosphorus. Electrochimica Acta 2011;56:9831–7.
[53] Park S, Woo TG, Jeon WY, Park HH, Lee MH, Bae TS, Seol KW. Surface characteristics of titanium anodized in the four different types of electrolyte. Electrochimica Acta 2007;53:863–70.
[54] Simka W, Iwaniak A, Nawrat G, Maciej A, Michalska J, Radwaski K, Gazdowicz J. Modification of titanium oxide layer by calcium and phosphorus. Electrochimica Acta 2009;54:6983–8.
[55] Matykina E, Arrabal R, Mohedano M, Pardo A, Merino MC, Rivera E. Stability of plasma electrolytic oxidation coating on titanium in artificial saliva. Journal of Materials Science Materials in Medicine 2013;24:37–51.
[56] Baszkiewicz J, Krupa D, Mizera J, Sobczak JW, Bilinski A. Corrosion resistance of the surface layers formed on titanium by plasma electrolytic oxidation and hydrothermal treatment. Vacuum 2005;78:143–7.
[57] Krząkała A, Służalska K, Widziołek M, Szade J, Winiarski A, Dercz G, Kazek A, Tylko G, Michalska J, Iwaniak A, Osyczka AM, Simka W. Formation of bioactive coatings on a Ti–6Al–7Nb alloy by plasma electrolytic oxidation. Electrochimica Acta 2013;104:407–24.
[58] Krząkała A, Służalska K, Widziołek M, Szade J, Winiarski A, Dercz G, Kazek A, Tylko G, Michalska J, Iwaniak A, Osyczka AM, Simka W. Characterization of bioactive films on Ti–6Al–4V alloy. Electrochimica Acta 2013;104:425–38.
[59] Kang BS, Sul YT, Oh SJ, Lee HJ, Albrektsson T. XPS, AES and SEM analysis of recent dental implants. Acta Biomaterialia 2009;5:2222–9.
[60] Jarmar T, Palmquist A, Bränemark R, Hermansson L, Engqvist H, Thomsen P. Characterization of the surface properties of commercially available dental implants using scanning electron microscopy, focused ion beam, and high-resolution transmission electron microscopy. Clinical Implant Dentistry and Related Research 2008;10:11–22.
[61] Oyane A, Kim HM, Furuya T, Kokubo T, Miyazaki T, Nakamura T. Preparation and assessment of revised simulated body fluids. Journal of Biomedical Materials Research Part A 2003;65:188–95.
[62] Cushnie EK, Khan YM, Laurencin CT. Amorphous hydroxyapatite-sintered polymeric scaffolds for bone tissue regeneration: physical characterization studies. Journal of Biomedical Materials Research Part A 2008;84:54–62.
[63] Sakhno Y, Bertinetti L, Iafisco M, Tampieri A, Roveri N, Martra G. Surface hydration and cationic sites of nanohydroxyapatites with amorphous or crystalline surfaces: a comparative study. Journal of Physical Chemistry C 2010;114:16640–8.
[64] Utomo WB, Donne SW. Transition metal inhibition of titanium corrosion: electrochemical behaviour of titanium in alkaline electrolyte. In: Proceedings of the Honolulu PRiME 2012. 2012., ISBN 978-1-62276-625-3.
[65] Hafez HS, Selim EMN, Kamel Eid FH, Tawfik WA, Al-Ashkar EA, Mostafa YA. Cytotoxicity, genotoxicity, and metal release in patients with fixed orthodontic appliances: a longitudinal *in vivo* study. American Journal of Orthodontics and Dentofacial Orthopaedics 2011;140:298–308.
[66] Gnedenkov SV, Sinebryukhov SL. Electrochemical impedance spectroscopy of oxide layers on the titanium surface. Russian Journal of Electrochemistry 2005;41:858–65.
[67] Messer RLW, Seta F, Mickalonis J, Brown Y, Lewis JB, Wataha JC. Corrosion of phosphate-enriched titanium oxide surface dental implants (TiUniteVR) under in vitro inflammatory and hyperglycemic conditions. Journal of Biomedical Materials Research Part B: Applied Biomaterials 2010;92:525–34.
[68] Gnedenkov SV, Sinebryukhov SL, Sergienko VI. Electrochemical impedance simulation of a metal oxide hetero structure/electrolyte interface: a review. Russian Journal of Electrochemistry 2006;42:197–211.